QUANTIFYING UNCERTAINTIES OF SPACE OBJECTS CENTROID POSITION BASED ON OPTICAL OBSERVATION

Zhuangbin Tan, Yang Yang, Yan Zhang, Xin Zhang, Bin Lin

School of Aeronautics and Astronautics, Sun Yat-Sen University, China
Email:tanzhb6@mail2.sysu.edu.cn, yiyinfeixiong@gmail.com, zhangyan25@mail.sysu.edu.cn
zhangx639@mail2.sysu.edu.cn, linb27@mail2.sysu.edu.cn

ABSTRACT

As the number of space debris continues to increase, which affects the normal space exploration activities, so we need to monitor and track the space targets. For space targets, the main detection method is to use optical sensor. This work aims to simulate the process of optical sensor observing the space objects and analyze the uncertainties of the centroid position of the space targets in both pixel coordinate system and spherical coordinate system. Our innovation lies in the estimation method of the centroid positions of the space targets. Specifically, we propose new hybrid algorithms by combining the Maximum Likelihood Estimation and the Levenberg Marquardt optimization methods, which enables more accurate estimation of the centroid position.

1 INTRODUCTION

For the observation of space targets, there are mainly two methods: ground-based and space-based. The main characteristics of ground-based observation is not restricted by factors such as volume and quality, which can achieve high spatial resolution and the far observation distance. But in the actual process of detection, due to the large distance between the ground station and space targets, there are some problems such as inability to full coverage for space targets, poor real-time monitoring and limited detection capabilities for small and medium-sized debris. Compared with the ground-based observation, space-based observation has obvious advantages in terms of spatial coverage and timeliness of monitoring.

In the space-based observation system, the observation information of the space objects can be obtained through the optical measurement. Common optical sensors include CCD (Charged Couple Device) or CMOS (Complementary Metal Oxide Semiconductor) cameras. For optical sensors, there are two observation modes: the star gaze mode and the target gaze mode. For the star gaze mode, where the optical camera is primarily focused on the star, the targets appear as streaks in the image. For the target gaze mode, the pointing of optical camera will synchronously move along the space observation target and the space target will be displayed as the point source on the optical camera. Our work mainly focuses on the research of target gaze mode.

At present, there is much related research on optical detection of space targets. In terms of detection noise, it mainly includes background noise and the noise of the optical instrument itself. Reference [1] mainly analyzed and modelled the noise of optical instrument itself. Reference [2] also analyzed and eliminated the possible background noise. Neither of the two references consider the evaluation and analysis of the total size of the intensity noise. In terms of determining the position of the space target, reference [3] mainly estimated the centroid positions of the space targets. Reference [4] considered the calculation and analysis of the centroid uncertainty of the space target position in the pixel coordinate system, but did not consider the centroid uncertainty of the target position in the spherical coordinate system.

So, by space-based observation platform, our research focuses on estimating the centroid position uncertainties of space targets in the both pixel coordinate system and spherical coordinate system for a given level of intensity noise variance.

The paper is organized as follows: in the second section, we describe the working process of the optical sensor (CCD or CMOS) and generate the optical signal intensity. In the third section, we carry out Gaussian fitting for optical signals of space targets to calculate the centroid position and analyze the uncertainty of the space target in the both pixel coordinate and spherical coordinate systems. In the fourth section, we describe the simulation results. The conclusions are drawn in the fifth section.

2 OPTICAL SIGNAL MODEL

2.1 Optical Signal

An optical sensor is a kind of sensor to measure the intensity of incident light. The light can directly come from an actively illuminated source, such as star, or be reflected off another object before the detector can measure. These objects are called passively illuminated objects because the light comes from the actively illuminated source is duplicate with above, but is reflected by a space target that is not radiating. The irradiance of passively illuminated object depends on the

amount of light incident on the reflecting source, which depends on the brightness of the light source. For space targets orbiting the earth, the main source of the light mainly is the sun.

When the radiation flux of the sun is incident on the opaque surface of the object region A, part of the signal is reflected. Referring to Eq. 1, the expected radiation flux density $I(\lambda)$ generated by the reflection received at the distance from the surface. It is related to the surface area of the target (A), the distance (r), the reflection phase function (ψ) and the standard expected radiant flux density $\left(I_{0\lambda,sun}\right)$ from the earth to the sun.

$$I(\lambda) = \int I_{0\lambda,sun} \frac{A}{r^2} \psi(\lambda) d\lambda \tag{1}$$

The expected signal intensity can be further determined as shown in Eq. 2:

$$S = \int (D-d) \frac{\lambda}{hc} e^{-\tau(\lambda)R(\zeta)} I(\lambda) d\lambda \tag{2}$$

which is composed of various factors such as the aperture area (D), the area of the aperture obscured (d), Planck constant (h), speed of light (c), atmospheric extinction coefficient (τ) and atmospheric function (R) related to the zenith angle (ζ).

2.2 Optical Observation

When the radiation flux of sun is incident on the opaque surface of the space object, part of the signal is reflected into the optical sensor. An optical camera receiving reflection signals from space targets can generate photons, release electrons, produce voltage and finally form the digital signals by the electric switch count [2]. Digital signal will form a signal image output on the optical camera. The whole process is shown in Fig 1.

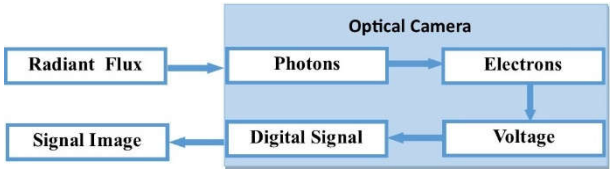

Figure 1. Working Flow of an Optical Camera

Every process generates different types of detection noises, such as the celestial and sky background noise (S_s), dark current noise (S_D), truncation noise (U) and read noise (S_R). Further, target pixel signals $\left(S_{obj}\right)$ can be calculated via Eq. 3 by the total intensity signal (S), the background noise (N_B) and the number of background pixels (n_B) used for detection.

$$S_{obj} = S - S_D - U - S_R - \left(S_s - \frac{N_B}{n_B}\right) \tag{3}$$

3 QUANTIFYING UNCERTAINTIES

3.1 Signal Fitting

Due to the defocusing effect of the observation camera, the imaging radius of the space target spreads to multiple pixels. Generally, it can be considered that the signal intensity distribution of space target imaging conforms to a two-dimensional Gaussian distribution centered on (x_0, y_0). So, for the optical signal, it can be fitted by the Gaussian curve, as shown in Eq. 4. Assumed that the actual position of the point source corresponds to the centroid of the fitted Gaussian curve [5], the actual position of the source can be obtained.

$$\mathrm{G} = Ae^{-\frac{1}{2}c_1(x-x_0)^2 - c_3(x-x_0)(y-y_0) + \frac{1}{2}c_2(y-y_0)^2} \tag{4}$$

In Eq. 4, A is the amplitude of the Gaussian curve, c_1 and c_2 define the size of the fitted Gaussian function on the x and y axis, c_3 orients the Gaussian function relative to the x and y axis. x_0 and y_0 are in the centroid position of the Gaussian distribution in the image.

For the aforementioned Gaussian fitting, there are mainly some optimization methods such as the Levenberg Marquardt algorithm (LM) and Maximum Likelihood Estimation (MLE) algorithm [3], referring to Appendix B-C for detail. To estimate the centroid position (x_0, y_0) of space target, the Center of Gravity (CG) method referring to Appendix A can also be used.

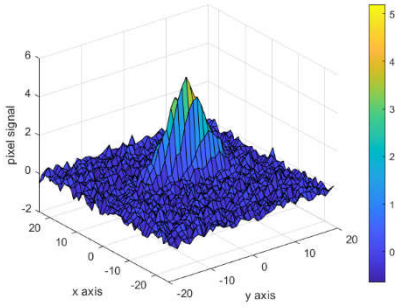

Figure 2. Raw Signal of Space Target

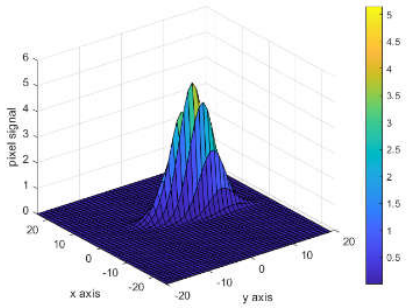

Figure 3. Gaussian Fitting Signal by LM

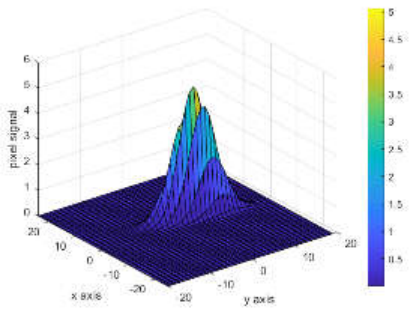

Figure 4. Gaussian Fitting Signal by MLE

For a space target with the intensity noise variance of 0.1 and a signal intensity of 5 in the pixel coordinate system, as shown in Fig 2, the Levenberg Marquardt and the Maximum Likelihood Estimation methods can be used for Gaussian parameters fitting. The fitting results are shown in Figs 3 and 4.

At the same time, we consider the possible shortcomings of Least Marquardt and Maximum Likelihood estimation. The limitation of Levenberg Marquardt optimization is the dependence on the choice of the initial centroid. For Maximum Likelihood Estimation, because the intensity noise itself is difficult to be completely modelled, there is certain error in the centroid position estimation. Based on this, we consider a new hybrid algorithm (MLE-LM) by combining the Maximum Likelihood Estimation and the Least Marquardt optimization. More specific meaning of MLE-LM, Maximum Likelihood Estimation mainly provides an initial estimation of the centroid parameters, and Least Marquardt optimization performs further optimization. LM-MLE is similar with it. The optimization results are similar with Figs 3 and 4.

3.2 Centroid Position Uncertainty

The uncertainty of the centroid position of the space target includes the calculation of the pixel coordinate system and the spherical coordinate system.

1) Uncertainty in the Pixel Coordinate System

According to the parameter set $\theta = (A, x_0, y_0, c_1, c_2, c_3)$ of the Gaussian curve fitted by the above optimization method, the maximum likelihood function (l) value can be calculated, referring to Eq. 17 in Appendix B.

Then we calculate the Fisher Information Matrix [6], shown in Eq. 5:

$$F(\theta) = E\left[\frac{\partial^2 l}{\partial^2 \theta_i \theta_j}\right] \tag{5}$$

where E is the expected value with respect to the likelihood function.

Finally, the exact Fisher Information Matrix (F) will be used to calculate the covariance matrix of the centroid position through Eq. 6.

$$K = F^{-1}(\theta) \tag{6}$$

2) Uncertainty in the Spherical Coordinate System

The coordinate conversion from the pixel coordinate system to the spherical coordinate system, the steps are shown in Fig 5.

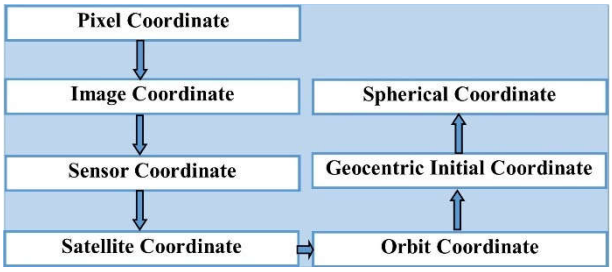

Figure 5. Coordinate Conversion from Pixel Coordinate to Spherical Coordinate

The centroid position (x_0, y_0) of the space target in the pixel coordinate system can be obtained by the above-mentioned fitting method, and the unit vector of the space target in the sensor coordinate system can be obtained by using three stars or satellites with known spatial positions and the calculation formula of the star angular distance [7] by Eq. 7:

$$\cos e_i = l_i \times x + m_i \times y + n_i \times z \tag{7}$$

where $\cos e_i$ can be calculated from the pixel positions of the target to be measured and known stars or satellites.

(l_i, m_i, n_i) and (x, y, z) are the unit vector of the sensor spatial positions of the known stars and the target to be measured, respectively.

The space target vector in the sensor coordinate system obtains the angular information (right ascension and declination angles) in the spherical coordinate system through coordinate transformation [8]. The detailed transformation formulas can also be found in Appendix D.

The centroid position uncertainty of the space target in the pixel coordinate system is converted to that in the spherical coordinate system through a simplified linearization rule shown in Eq. 8:

$$K_{\alpha,\delta} = \frac{\partial[\alpha\ \ \delta]^T}{\partial[x_0\ y_0]^T} K_{x_0,y_0} \left[\frac{\partial[\alpha\ \ \delta]^T}{\partial[x_0\ \ y_0]^T}\right]^T \tag{8}$$

where P_{x_0,y_0} is the variance matrix of the centroid position in the pixel coordinate system; α *and* δ represent the right ascension and declination of the spherical coordinate system, respectively.

4 SIMULATION RESULTS

Based on understanding the positioning principle of the target to be measured, we can simplify the process and use known satellites as background stars to solve the angle measurement information of the space targets which will be measured. We simulate and generate 7 space targets, of which 3 targets are known space targets and 4 space targets will be measured. The angle(α, δ) and radius(r) information in spherical coordinate system is shown in Table 1 where Scm is the position of the optical sensor in the spherical coordinate system.

Table 1. Initial Parameters of Simulation Space Targets

Target No	α(°)	δ(°)	$r(km)$
S1	43.98	57.43	41598
S2	66.42	77.47	41001
S3	83.71	-18.46	40505
S4	101.56	-49.17	40004
S5	158.53	16.13	42000
S6	121.67	-89.24	39509
S7	151.67	-61.24	39000
Scm	20	20	42016

Through coordinate transformation and projection transformation, every space target forms a light spot in a 4k × 4k pixel plane. Due to the defocusing effect of the optical camera, every target occupies 11×11 pixels. The intensity signal (E_m) of each point can be calculated by referring to [9]. If the space target is a cuboid, the corresponding expression is showed in Eq. 9:

$$E_m = \frac{E_s}{\pi R^2} lw\rho cos(\alpha_1) cos(\alpha_2) \tag{9}$$

where E_s indicates the direct sun illuminance received by the spacecraft R is the distance from the space target to the optical sensor, l and w indicate the length and width of the space target, respectively, ρ is the diffuse reflectance, α_1 and α_2 are defined as the incident angle and reflection angle of sun light, respectively.

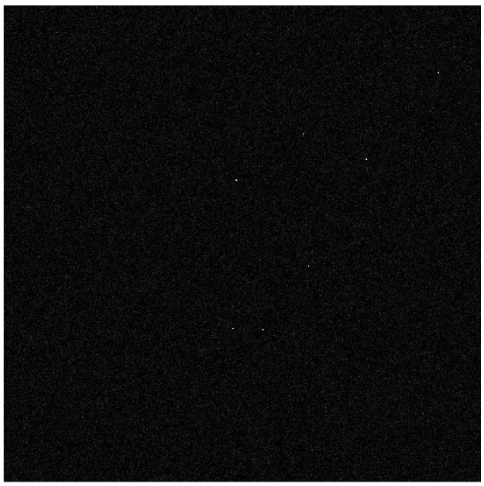

Figure 6. Simulated Image from Optical Sensor

For a simple assessment of the magnitude of light intensity, Eq. 9 can be simplified to only depend on distance. A total intensity noise with a variance of 0.1 and focal length (f) of 500 mm are applied. Finally, the star map result is shown in Fig 6.

4.1 Centroid Position Estimation

We will sample 1000 times and average the calculated centroid points (x_0, y_0). At the same time, we use the Eq. 9 and Eq. 10 to evaluate the optimization performance of different optimization algorithms:

$$l_{x_0} = \frac{1}{n}\sum_{i=1}^{n}(x_0 - x_m)^2 \tag{10}$$

$$l_{y_0} = \frac{1}{n}\sum_{i=1}^{n}(y_0 - y_m)^2 \tag{11}$$

where n is the number of samples. (x_m, y_m) is the true centroid position of the space target, (x_0, y_0) is the estimated centroid position of the space target.

The simulation results are obtained through calculation, and average values $(\overline{x_0}, \overline{y_0})$of the centroid positions of the 4 targets to be measured are shown in Table 2.

Table 2. Average Value of Centroid Position by Different Algorithms

Target No	$\binom{x_m}{y_m}$	$(\overline{x_0}, \overline{y_0})$				
		MLE-MLE	LM-LM	MLE-LM	LM-MLE	CG
S1	(2777.7, 1970.9)	(2778.0, 1971.0)	(2778.1, 1971.1)	(2778.0, 1971.0)	(2778.0, 1971.0)	(2178.0, 1971.0)
S2	(2785.7, 2224.9)	(2786.0, 2225.0)	(2786.1, 2225.1)	(2786.0, 2225.0)	(2786.0, 2225.0)	(2786.0, 2225.0)
S3	(1504.3, 2000.0)	(1504.0, 2000.0)	(1504.1, 2000.1)	(1504.0, 2000.0)	(1504.0, 2000.0)	(1504.0, 2000.0)
S4	(1107.0, 2570.0)	(1107.0, 2570.0)	(1107.1, 2570.1)	(1107.0, 2570.0)	(1107.0, 2570.0)	(1107.0, 2570.0)

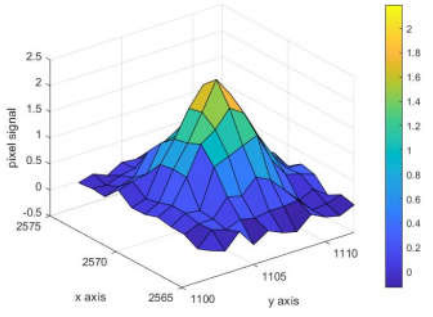

Figure 7. Raw Signal of Space Target S4

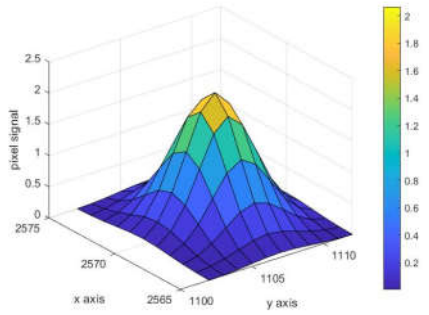

Figure 8. Gaussian Fitting Signal of Space Target S4 by MLE-LM Method

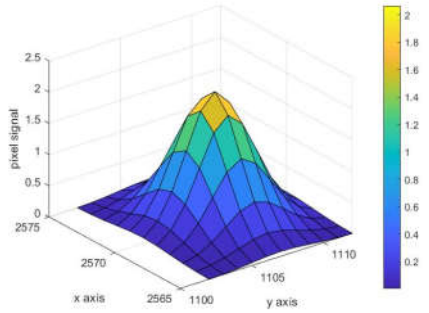

Figure 9. Gaussian Fitting Signal of Space Target S4 by LM-MLE Method

For example, for the Gaussian fitting of space target S4, the optimization results by the new hybrid algorithm (MLE-LM or LM-MLE) are shown in Fig 8 and Fig 9.

It can be seen from the Figs. 8 and 9 that the mixed algorithms (MLE-LM or LM-MLE) can fit the signal intensity well. The results of other optimization methods are similar with the above results.

Of course, we also compared the performance of different optimization methods, which are shown in the table 3.

Table 3. The Comparison by Different Optimization Methods

Target No	(l_{x_0}, l_{y_0})				
	MLE-MLE	LM-LM	MLE-LM	LM-MLE	CG
S1	(0.102, 0.102)	(0.139, 0.139)	(0.096, 0.096)	(0.096, 0.096)	(0.098, 0.005)
S2	(0.073, 0.073)	(0.106, 0.106)	(0.066, 0.066)	(0.066, 0.066)	(0.182, 0.241)
S3	(0.075, 0.075)	(0.074, 0.074)	(0.073, 0.073)	(0.073, 0.073)	(0.078, 0.002)
S4	(0.003, 0.003)	(0.017, 0.017)	(0.003, 0.003)	(0.003, 0.003)	(0.002, 0.001)

It can be seen from Table 3 that in general, the hybrid optimization algorithm yields slightly more accurate in estimating the centroid position of the space target.

4.2 Centroid Position Uncertainty

In the pixel coordinate system, the average uncertainty (P_{x_0,y_0}) of the centroid of the space target can be obtained by calculating the Fisher Information Matrix and standard variance. The results are shown in the Table 4.

Table 4. The Average Uncertainty of Centroid Position in Pixel Plane Space by Different Optimization

Target No	(P_{x_0,y_0})/pixel			
	MLE-MLE	LM-LM	MLE-LM	LM-MLE
S1	(6.55e-5, 6.59e-5)	(6.44e-5, 6.67e-5)	(6.52e-5, 6.62e-5)	(6.52e-5, 6.52e-5)
S2	(1.37e-4, 1.39e-4)	(1.33e-4, 1.39e-4)	(1.37e-4, 1.39e-4)	(1.37e-4, 1.39e-4)
S3	(1.82e-4, 1.83e-4)	(1.77e-4, 1.84e-4)	(1.80e-4, 1.84e-4)	(1.80e-4, 1.84e-4)
S4	(2.91e-4, 2.94e-4)	(2.85e-4, 2.96e-4)	(2.90e-4, 2.96e-4)	(2.92e-4, 2.96e-4)

According to Eq. 26 in the Literature [4], we can find that there is a relationship between the uncertainty of the centroid position and the variance of the noise in the pixel coordinate system.

The centroid position uncertainty of the space target in the pixel coordinate system is converted to that in the spherical coordinate system by Section 3.2. The results are shown in Table 5.

Table 5. The Average Uncertainty of Centroid Position in Spherical Coordinate by Different Methods

Target No	$P_{\alpha,\delta}('')$			
	MLE-MLE	LM-LM	MLE-LM	LM-MLE
S1	(0.95, 0.57)	(0.94, 0.58)	(0.95, 0.58)	(0.95, 0.58)
S2	(2.60, 1.41)	(2.56, 1.39)	(2.60, 1.41)	(2.60, 1.41)
S3	(1.97, 1.02)	(1.96, 1.02)	(1.97, 1.02)	(1.97, 1.02)
S4	(2.83, 1.23)	(2.86, 1.21)	(2.86, 1.23)	(2.86, 1.23)

5 CONCLUSION

By adding a certain magnitude of intensity noise, the star map simulation of space targets can reflect the actual optical detection process. Through the simulation results, we find that both Levenberg Marquardt algorithm and Maximum Likelihood Estimation algorithm can estimate the centroid positions of the space targets very well. In the pixel coordinate system, the error of the centroid position estimation will not exceed 0.5 pixel. From the analysis of the performance indicators of optimization method, we find that the hybrid methods of combining the Maximum Likelihood Estimation and Levenberg Marquardt algorithm yields slightly more accurate centroid position estimates.

At the same time, we find that in the pixel coordinate system, for the uncertainties of the centroid position of the space targets, the results reach the order of 10^{-5}-10^{-4} pixel. In the spherical coordinate system, the uncertainty estimation results of the centroid position of the space targets are about the order of $1'' - 2''$, which is basically equivalent to the actual uncertainty.

We have proposed new hybrid algorithms by combining the Maximum Likelihood Estimation and Levenberg Marquardt algorithm. To a certain extent, it is more accurate to estimate the centroid position of the space target.

6 ACKNOWLEDGMENTS

This work has been funded by the Shenzhen Science and Technology Program Grant No. KQTD20190929172704911. and Guangdong Basic and Applied Basic Research Foundation Project (No. 2020A1515110216).

Appendix A. Center of Gravity

The calculation of the center of gravity method which is known as the moment method is shown in Eq. 13.

$$(x_0, y_0) = \left(\frac{\sum_{ij} I_{ij} x_{ij}}{\sum_{ij} I_{ij}}, \frac{\sum_{ij} I_{ij} y_{ij}}{\sum_{ij} I_{ij}}\right) \tag{13}$$

Appendix B. Maximum Likelihood Estimation

According to Eq. 4, the intensity signal of optical sensor CCD or CMOS is assumed to be fitted by Gaussian curve. Define the likelihood of the parameter set θ of the signal as Eq. 14.

$$\mathrm{L} = P(S = G|\theta) \tag{14}$$

Then the maximum of likelihood is defined as Eq. 15.

$$\hat{\theta}_{MLE} = argmax_{\theta}\big(P(S = G|\theta)\big) \tag{15}$$

If the noise of two different pixels is Gaussian independent, the likelihood is shown as in Eq. 16:

$$L = \prod_{i}^{n_{pix}} exp\left(-\frac{1}{2}\left(\frac{(S_i - G_i)^2}{\sigma_i^2}\right)\right) \tag{16}$$

where G_i is the Gaussian surface, the ith pixel signal is defined as S_i, σ_i is the standard deviation of the noise distribution at pixel i.

Then the log likelihood can be expressed as Eq. 17.

$$l = -\sum_{i}^{n_{pix}} \frac{\big(S_i - G_i(\theta)\big)^2}{2\sigma_i^2} \tag{17}$$

From the log-likelihood function l, its gradient and the Hessian matrix can be obtained by Eq. 18 and 19, respectively.

$$\nabla l = \left(\frac{\partial l}{\partial A}, \frac{\partial l}{\partial x_0}, \frac{\partial l}{\partial y_0}, \frac{\partial l}{\partial c_1}, \frac{\partial l}{\partial c_2}, \frac{\partial l}{\partial c_3}\right) \tag{18}$$

$$H = \begin{bmatrix} \frac{\partial^2 l}{\partial^2 A} & \frac{\partial^2 l}{\partial A \partial x_0} & \frac{\partial^2 l}{\partial A \partial y_0} & \frac{\partial^2 l}{\partial A \partial c_1} & \frac{\partial^2 l}{\partial A \partial c_2} & \frac{\partial^2 l}{\partial A \partial c_3} \\ \frac{\partial^2 l}{\partial x_0 \partial A} & \frac{\partial^2 l}{\partial^2 x_0} & \frac{\partial^2 l}{\partial x_0 \partial y_0} & \frac{\partial^2 l}{\partial x_0 \partial c_1} & \frac{\partial^2 l}{\partial x_0 \partial c_2} & \frac{\partial^2 l}{\partial x_0 \partial c_3} \\ \frac{\partial^2 l}{\partial y_0 \partial A} & \frac{\partial^2 l}{\partial y_0 \partial x_0} & \frac{\partial^2 l}{\partial^2 y_0} & \frac{\partial^2 l}{\partial y_0 \partial c_1} & \frac{\partial^2 l}{\partial y_0 \partial c_2} & \frac{\partial^2 l}{\partial y_0 \partial c_3} \\ \frac{\partial^2 l}{\partial c_1 \partial A} & \frac{\partial^2 l}{\partial c_1 \partial x_0} & \frac{\partial^2 l}{\partial c_1 \partial y_0} & \frac{\partial^2 l}{\partial^2 c_1} & \frac{\partial^2 l}{\partial c_1 \partial c_2} & \frac{\partial^2 l}{\partial c_1 \partial c_3} \\ \frac{\partial^2 l}{\partial c_2 \partial A} & \frac{\partial^2 l}{\partial c_2 \partial x_0} & \frac{\partial^2 l}{\partial c_2 \partial y_0} & \frac{\partial^2 l}{\partial c_2 \partial c_1} & \frac{\partial^2 l}{\partial^2 c_2} & \frac{\partial^2 l}{\partial c_2 \partial c_3} \\ \frac{\partial^2 l}{\partial c_3 \partial A} & \frac{\partial^2 l}{\partial c_3 \partial x_0} & \frac{\partial^2 l}{\partial c_3 \partial y_0} & \frac{\partial^2 l}{\partial c_3 \partial c_1} & \frac{\partial^2 l}{\partial c_3 \partial c_2} & \frac{\partial^2 l}{\partial^2 c_3} \end{bmatrix} \tag{19}$$

Applying these functions to a nonlinear optimization program (such as Newton iteration) to solve the parameter set θ, it can be calculated in detail by Eq. 20.

$$\theta^{(k+1)} = \theta^{(k)} - \big(H^{(k)}\big)^{-1} \nabla l^{(k)} \tag{20}$$

Where a superscript (k) indicates the iteration index and $H^{(k)}$ is the Hessian matrix of l evaluated at $\theta^{(k)}$.

Appendix C. Levenberg Marquardt Method

The Levenberg Marquardt method fits the Gaussian function through all the data points of the window. The problem of minimizing with Levenberg Marquardt is shown by Eq. 21:

$$\min F(\theta) = \frac{1}{2} \sum_{i=1}^{n_{pix}} \big(f_i(\theta)\big)^2 \tag{21}$$

$$f_i = S_i - G_i \tag{22}$$

where $\theta = (A, x_0, y_0, c_1, c_2, c_3)$ is the vector of parameters to be determined n_{pix} is the number of signal pixels, S_i is the intensity value of the ith pixel. G_i is the function to be fitted through the data, which is defined as Eq. 4.

Then, the matrix obtained by the first-order partial derivative of the function f_i is the Jacobian matrix

$$\big(J(x)\big)_{ij} = \frac{\partial f_i}{\partial x_i}(x) \tag{23}$$

Finally, the definition of step size h_{lm} is obtained by solving Eq. 24.

$$(J^T J + \mu I) h_{lm} = -g \tag{24}$$
$$with\ g = J^T f\ and\ \mu \geq 0$$

Here, μ is defined as damping parameter and I is identity

matrix.

The update of parameter set (θ) can be calculated in Eq. 25.

$$\theta^{(k+1)} = \theta^{(k)} + h_{lm} \tag{25}$$

Appendix D. Coordinate Conversion

After the target position $(\boldsymbol{r})$ of the inertial coordinate system is rotated and translated by Eq. 26, the target position $(\boldsymbol{r}_o)$ in the orbital coordinate system is obtained.

$$\boldsymbol{r}_o = \boldsymbol{B}\boldsymbol{R}_{ECI}^{orbit}\boldsymbol{r} + \boldsymbol{c} \tag{26}$$

In Eq. 26, $\boldsymbol{B}$ is the adjustment matrix of coordinate axis, $\boldsymbol{R}_{ECI}^{orbit} = \boldsymbol{R}_z(u)\boldsymbol{R}_x(i)\boldsymbol{R}_z(\Omega)$, i is the orbital inclination, Ω is the ascending node right ascension, u is latitude angle. $\boldsymbol{c}$ is the offset.

The target position $(\boldsymbol{r}_o)$ in the orbital coordinate system is rotated by the satellite attitude angle to obtain the position $(\boldsymbol{r}_s)$ in the satellite coordinate system. The specific expression is represented by Eq. 27:

$$\boldsymbol{r}_s = \boldsymbol{R}_{orbit}^{sat}\boldsymbol{r}_o \tag{27}$$

where $\boldsymbol{R}_{orbit}^{sat} = R_x(\psi)R_y(\gamma)R_z(\phi)$, ψ, γ and ϕ indicate the roll angle, pitch angle and yaw angle of the satellite, respectively.

The target position $(\boldsymbol{r}_s)$ in the satellite coordinate system is rotated by the sensor pointing angle, and the position $(\boldsymbol{r}_c)$ in the sensor coordinate system is obtained through Eq. 28.

$$\boldsymbol{r}_c = \boldsymbol{R}_{sat}^{cam}\boldsymbol{r}_s \tag{28}$$

In Eq.28, $\boldsymbol{R}_{sat}^{cam} = \boldsymbol{R}_y\left(\frac{\pi}{2} - \varepsilon\right)\boldsymbol{R}_z(\alpha)$, α and ε indicate the azimuth and pitch angle of the sensor, respectively.

REFERENCE

1. Mikhail Konnik, James Welsh. High-level Numerical Simulations of Noise in CCD and CMOS Photosensors: review and tutorial. 2014.
2. Francois Sanson, Carolin Frueh. Noise Estimation and Probability of Detection in Non-resolved Images: Application to Space Object Observation. Advances in Space Research. 64, 1432-1444. 2019.
3. Tjorven Delabie, Joris De Schutter, Bart Vandenbussche. An Accurate and Efficient Gaussian Fit Centroiding Algorithm for Star Trackers. Journal of the Astronautical Sciences. 61, 60-84. 2019.
4. Francois Sanson, Carolin Frueh. Quantifying Uncertainties in Signal Position in Non-resolved Object Image: Application to Space Object Object Observation. Advance in Space Research. 2019.
5. Patrick M. Kelly. Optical Astrometry and Orbit Determination (D). 2020.
6. Nathan Hagen, Eustace L. Dereniak. Gaussian Profile Estimation in Two Dimension. Applied Optical. Vol. 47, No. 36. 2008.
7. Lei Zhang, Xin He, Zhong-hui He, Jing-ming Guo. Fast Celestial Positioning for Space Objects Based on Star Identification in Chinese. Optical and Precision Engineering. Vol 22, No 11. 2014.
8. Wei-dong Sheng, Yang Xu, Yi-yu Zhou, Wei An. Analysis of LOS Measurement Error for Space-Based Optical Sensor in Chinese. Journal of Astronautics. Vol. 32, No. 1. 2011.
9. Qin Yang, Sui Song, Yanxin Ma, Min Lu, Jun Zhang. Design and Implement of Space-Based Target Imaging Simulation System in Chinese. Laser & Optoelectronics Progress. Vol. 111, No. 101. 2015.